Hindawi
Journal of Spectroscopy
Volume 2017, Article ID 5473874, 10 pages
https://doi.org/10.1155/2017/5473874

Research Article

Kinetic Study of Atmospheric Pressure Nitrogen Plasma Afterglow Using Quantitative Electron Spin Resonance Spectroscopy

A. Tálský, O. Štec, M. Pazderka, and V. Kudrle

Department of Physical Electronics, Masaryk University, Kotlarska 2, 61137 Brno, Czech Republic

Correspondence should be addressed to V. Kudrle; kudrle@sci.muni.cz

Received 14 September 2016; Revised 18 November 2016; Accepted 28 November 2016; Published 19 March 2017

Academic Editor: Nikša Krstulović

Quantitative electron spin resonance spectroscopy is used to measure nitrogen atom density in atmospheric pressure dielectric barrier discharge afterglow. The experiment shows that oxygen injection into early afterglow increases the nitrogen dissociation in certain parts of the afterglow while it is decreased in the rest of the afterglow. Numerical kinetic modelling supports and explains the experimental data while the best fit provides some a priori unknown parameters such as initial concentrations and rate constants.

1. Introduction

Nonequilibrium cold plasmas at atmospheric pressure and especially dielectric barrier discharges are getting increased attention of both basic and applied research. They are widely used in many industrial applications from ozone production [1] and lighting [2] to plasma surface modifications [3]. Their main advantages over other competing technologies are the ease-of-use, economy, and environmental considerations [4]. Besides the already established applications, there is rapid expansion of atmospheric pressure plasmas into new areas, such as plasma-chemical synthesis of substances which are difficult to attain by other techniques [5–7], plasma medicine [8], material disinfection and sterilisation [9], and use in cosmetics [10] or in fashion industry [11].

Nitrogen plasmas are often used as a source of high density nitrogen atoms. Molecular nitrogen is rather inert gas, but atomic nitrogen is quite reactive, which is made use of in plasma deposition of nitride films [12] or plasma nitridation [13]. Although the low pressure plasmas are currently dominating this field, there is strong incentive for research and development of nitrogen plasma sources operating at atmospheric pressure [14].

In order to develop new plasma-chemical technologies it is important to understand the elementary processes taking place in both the active plasma and plasma afterglow. Nitrogen, despite being a simple diatomic molecule, has quite complex plasma chemistry and kinetics, especially in mixtures with oxygen [15, 16]. As stated above, the nitrogen atoms play a significant kinetic role due to their high reactivity. Their concentration is then one of the most important parameters to be experimentally determined. Although there is broad range of experimental techniques able to detect N atoms, for example, optical emission spectroscopy, only few of them are suitable for absolute, not relative, measurements. UV absorption spectroscopy [17], NO titration [18], mass spectroscopy (MS) [19], laser induced fluorescence (LIF) [20], and catalytic probes [21], for example, are widely used. Another challenge is an operation of such diagnostic technique in atmospheric pressure, which, for example, greatly increases quenching in LIF, complicates pumping in MS, or totally changes the plasma chemistry (NO titration).

In this paper, the electron spin/paramagnetic resonance (ESR/EPR) [30–32] method is used for N atom density determination. This method is very useful for detection and identification of paramagnetic particles and especially radicals [33–35]. Although the method is routinely used in chemistry, its use in plasma physics is relatively rare. Since the pioneering works [36–38], other, mostly laser based methods appeared which are now considered mainstream.

Electron spin or paramagnetic resonance (ESR/EPR) is essentially microwave absorption spectroscopy [39] on

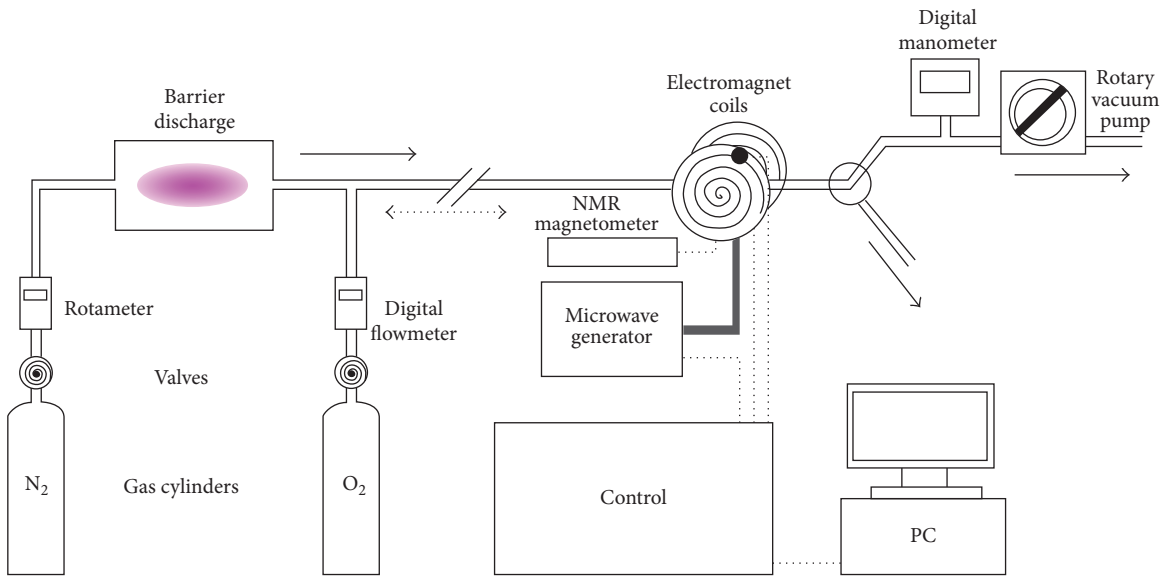

Figure 1: Schematic drawing of the experimental set-up.

Zeeman split [40] levels. The transitions with very low energy separation between the upper and the bottom levels (as is the case in microwave spectroscopy) are very easily disturbed by the collisions with other particles. The collisional/pressure broadening of absorption line can be quite pronounced [41, 42], especially for gas phase atomic and molecular lines with very low natural linewidths. This makes most of the species (for extensive list, see [43]), including, for example, atomic oxygen, difficult to detect in atmospheric pressure plasmas. However, the particles in s-state, such as nitrogen or hydrogen atoms in ground state, do not exhibit pressure broadening and can be detected by ESR/EPR even at atmospheric pressure.

There are a number of works, both theoretical and experimental, dealing with low pressure plasma diagnostics by ESR/EPR method [44–50]. However, due to above-mentioned difficulties of pressure broadening, the diagnostics of atmospheric pressure plasmas by EPR/ESR is rather unresearched topic, as our previous paper [51] is, to authors' best knowledge, still the only one published.

Although the nitrogen and oxygen plasmas are studied for very long time, there is still intensive research [52–54] going on. The discharges in N_2-O_2 mixtures have very complicated plasma kinetics and some effects, especially in mixtures with low O_2/N_2 ratio, are not fully explained yet. In our previous work [55] it was reported that adding of small amount of oxygen into a low pressure nitrogen plasma afterglow causes an increase of nitrogen atom density. In this paper we extend the study of the influence of oxygen admixture on the nitrogen afterglow to atmospheric pressure.

2. Experimental Apparatus and Methods

2.1. Experimental Set-Up. The experimental apparatus is depicted in Figure 1. Nitrogen plasma at atmospheric pressure was produced using industrial ozoniser LifeTech 50. It is based on coaxial dielectric barrier discharge, excited by 25–35 W power at 15 kHz frequency. The stainless steel inner electrode has approx. 2 cm diameter and is separated by 0.7 mm plasma gap and 2.5 mm thick corundum (Al_2O_3) ceramics from the outer electrode which is realised by an aluminium foil tightly wrapped around the ceramic tube. The discharge tube is approx. 15 cm long. Although the metal electrode in direct contact with plasma can significantly reduce N atom density in the effluent due to increased surface recombination/reassociation, this design [56] is well established in industrial ozonisers.

The discharge was operated in flowing (12 standard litres per minute) nitrogen, coming from pressurised cylinder (Messer-Griesheim, purity 99.995%) via pressure reduction valve. The volumetric flow rate of nitrogen was measured by flowmeter with floating element (rotameter UPLS-R3). Downstream from the plasma source, the oxygen is optionally introduced. The oxygen comes from pressurised cylinder (Messer-Griesheim, purity 99.995%) via Hastings mass flow-controller maintaining the oxygen flow at 7.5 sccm (standard cubic centimetre per minute). The tubing is made from polyethylene and stainless steel.

The oxygen is introduced into the afterglow tube just downstream from the plasma generator using an inlet three-way valve. This configuration permits presetting the oxygen flow on the flow-controller and rapidly switches on and off the oxygen admixture. The distance between the output port of the plasma generator and the inlet of oxygen is 6 cm. The afterglow tube is made of fused silica with 10 mm outer diameter and 8 mm inner diameter. This tube passes through ESR/EPR spectrometer resonator and ends in another outlet three-way valve. In normal operation the plasma afterglow vents into open atmosphere and the afterglow tube length (approx. 2.5 metres) together with high gas flow prevents any back-diffusion of air into the afterglow or plasma. In second position of this outlet valve the whole apparatus can be pumped down by the rotary vane oil vacuum pump. This is

used for calibration by molecular oxygen at reduced pressure and for degassing/cleaning as before every measurement series the whole plasma system is evacuated to pressure about 10 Pa to remove residual impurities. After that, the nitrogen flow is switched on and the outlet three-way valve is turned to normal position. Then the discharge is run 1 hour at maximum power to burn-in the plasma generator and remove the possible contamination off the electrode. Only after such procedure are the experiments started.

The distance from the inlet of oxygen admixture to the measuring ESR/EPR resonator can be changed by shifting the whole plasma system. To ease this, the plasma system including afterglow tube is placed on nonmagnetic rails parallel to ESR/EPR resonator axis. The furthest possible position is limited by the rail length to 90 cm. However, in the present study the maximum extension was not used as the ESR/EPR signal in this extreme position was already difficult to measure. The minimum distance in which the measure could be carried out is about 20 cm. Although it is mechanically possible to place the discharge closer to the resonator, at shorter distances the magnetic field of the ESR/EPR spectrometer electromagnet affected the plasma generator.

The ESR/EPR spectrometer JEOL JES-PE is specially adapted for use in plasma physics. It is classical continuous wave spectrometer [34] using klystron source operating at X band and with standard sensitivity around 10^{10} paramagnetic particles in the interaction volume of TE_{011} resonator. The output voltage of the analogue spectrometer is measured by digital voltmeter (Metra M1T390, 5 digits) and transmitted to a personal computer via GPIB. The ESR/EPR signal is analysed and postprocessed using custom software. It automatically identifies the spectral lines and calculates their peak-to-peak height, peak-to-peak width w, and area under the absorption line I_N (as ESR/EPR lines are typically [34] recorded in the form of derivation, double integration is needed).

2.2. The Principle of Measurement and Calibration Procedure. The ESR/EPR phenomenon is based on resonant absorption of microwave photons by transition between Zeeman split [40] energy levels. Typically, the resonance is achieved by variable magnetic field (which sets the energy level splitting) while the microwave frequency (i.e., photon energy) is fixed. The area under absorption spectral line is proportional [38] to the concentration of absorbing paramagnetic particles. The proportionality constant depends on spectrometer settings and the transition probability (Einstein coefficient). After a calibration of the spectrometer by a known sample it is possible to measure the concentration of paramagnetic particles absolutely [57].

In this work, the spectrometer calibration [44] is carried out using molecular oxygen O_2. The measuring resonator is filled with gaseous molecular oxygen at known concentration (calculated from pressure and temperature), its intensive spectral line C (the traditional naming, found in many papers, e.g., [38, 41, 43, 44]) is recorded, and corresponding double integral I_C is calculated. Using the same settings of the spectrometer, the ESR/EPR line of atomic nitrogen is recorded and its double integral I_N is calculated. Knowing the Einstein coefficients of both species the concentration of atomic nitrogen is given by simple relation

$$[N] = 5.88 \cdot 10^{-3} I_N / I_C \times [O_2].$$

The numeric constant in this formula is the ratio of Einstein coefficient of molecular oxygen line C and that of one component of atomic nitrogen triplet [43].

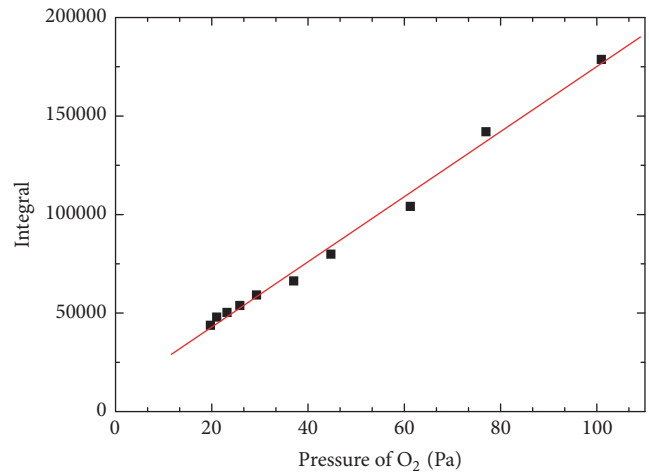

FIGURE 2: Calibration of EPR spectrometer using the line C of molecular oxygen. Linear dependency of absorption line integral I_C (i.e., double integral of measured signal) on oxygen pressure validates the calibration process and its slope provides a constant $[O_2]/I_C$ needed for the calibration.

As the oxygen calibration is carried out in the flow-regime, due to Hagen–Poiseuille law [58] there exist pressure gradients along the tube, making the pressure in the ESR/EPR resonator slightly different from the one indicated by pressure meter. The vacuum conductivity of the tube depends [59] on pressure, too. Moreover, as at low pressures the partial pressure of O_2 could be smaller than the total pressure indicated due to small vacuum leaks, finite base pressure of the pump used, or degassing from walls, it is better to record O_2 line for several indicated pressures than to rely on single value only. The result of such calibration measurement is shown in Figure 2.

The ESR/EPR lines of atomic nitrogen are extremely narrow and therefore sensitive to any broadening [41]. The ground state of nitrogen $N(^4S_{3/2})$ has zero orbital magnetic momentum and its paramagnetism is given only by the electron spin. In that case there should be no collision induced broadening; its spectral linewidth should be independent of pressure [60]. In work [61] this was studied in the pressure range from 50 to 600 Pa and in temperature range from 80 to 300 K. It was found that with decreasing temperature the apparent linewidth $w = 6\,\mu$T remained constant, while the integral and thus the concentration [N] decreased. The linewidth was thus independent of N atom density, which suggested that the role of spin-spin relaxation at these N concentrations (around 10^{13}–10^{14} cm^{-3}) is negligible.

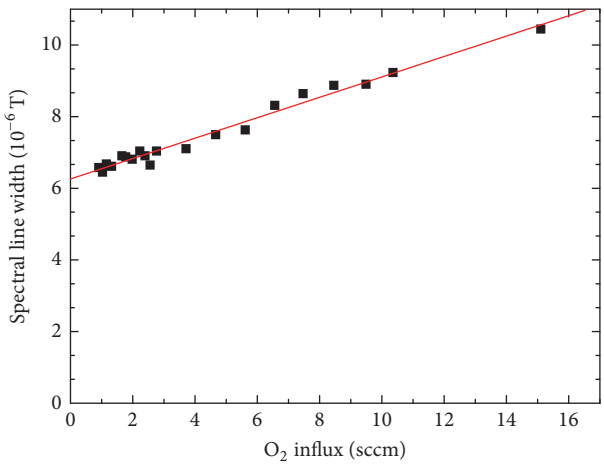

Figure 3: Linewidth of N atom ground state ($^4S_{3/2}$) EPR line as a function of oxygen admixture.

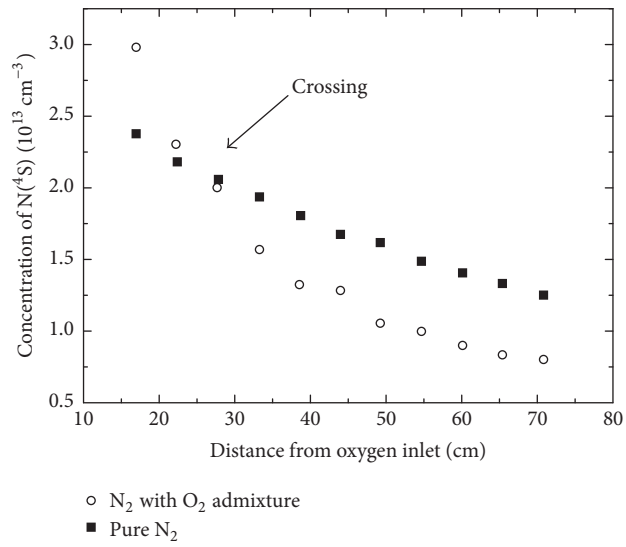

Figure 4: Spatial distribution of the nitrogen atom concentration (in ground state) along the afterglow tube for two cases: with and without 625 ppm oxygen admixture.

In present work, a similar measurement of N($^4S_{3/2}$) linewidth was carried out in pure nitrogen afterglow but at atmospheric pressure. Practically the same value $w = 6.4\,\mu$T was observed. The linewidth (and spectral line shape) being constant, the concentration of N atoms should be directly proportional to the absorption line height and by consequence also to the peak-to-peak height of the measured (i.e., absorption derivative) line. It can be advantageous to use this peak-to-peak height over the spectral line integral as the latter exhibits much higher statistical variations due to an increased influence of a noise overlaying the line shoulders.

However, a presence of other paramagnetic particles can affect even the s-states. The experimental result, nitrogen spectral linewidth as a function of molecular oxygen admixture, is shown in Figure 3. The changing nitrogen linewidth prevents the use of simple line height as concentration indicator and the integral must be used instead. This effect is consistent with [60].

3. Results and Discussions

3.1. Experimental Results. Electron paramagnetic/spin resonance was used to measure the concentration of atomic nitrogen N($^4S_{3/2}$) in atmospheric pressure discharge afterglow. This density [N] was measured along fused silica tube in pure nitrogen afterglow and with 625 ppm of oxygen injected into the early afterglow; see Figure 4.

The most important result is the fact that the two curves apparently intersect. It means that a small admixture of oxygen can cause both an increase and a decrease in concentration of nitrogen atoms, depending on which part of the afterglow is observed. This nontrivial behaviour is a typical demonstration of complexities inherent in N_2-O_2 kinetics.

In flowing kinetic studies, if the gas velocity is known, the spatial distribution of measured species can be transferred to their temporal evolution. Sometimes the same gas velocity in the whole cross-section (i.e., plug flow) is assumed without any further consideration. However, there can be a significant radial gradient of gas velocity due to a shear flow and a boundary layer. While a laminar flow in circular tube produces well-known parabolic velocity profile, in a well-developed turbulent flow the shear zone is thin compared to the tube diameter, so the plug flow is appropriate. The character of flow in a tube can be deduced from the Reynolds number [62]

$$R = ud/\nu,$$

where u is mean flow velocity, d is the inner tube diameter, and ν is cinematic viscosity. For nitrogen at standard pressure and temperature $\nu = 1.50 \cdot 10^{-5}\,\mathrm{m^2\,s^{-1}}$ according to [63], which gives $R = 2100$ for our experimental conditions. This value falls in critical Reynolds number range $R = 1800$–2300 where a transition between the laminar and the turbulent flow happens [64]. One can expect that the inhomogeneity caused by the lateral oxygen inlet together with other imperfections introduces some additional turbulence. Based on this reasoning, there is enough turbulence to consider the plug flow as a valid approximation in this paper, too.

In that case, the radially uniform flow velocity is approx. 4 m/s. Using this value, the measured dependence of the nitrogen atom density on position in the afterglow (Figure 4) was recalculated to the dependence on time; see Figure 5.

It is experimentally impossible to measure the concentration near the oxygen inlet (i.e., at times close to $t = 0$ s) as the T-piece (needed for the inlet) cannot pass through the ESR/EPR measuring resonator opening and the close distance between the plasma generator and the ESR/EPR electromagnet would magnetically influence the plasma generator and the plasma itself. However, if one excludes a back-diffusion, it is evident that with or without oxygen admixture the value at $t = 0$ s must be the same; that is, both curves must start at the same initial value depicted in Figure 5 by red circle. While this common initial value is a priori unknown

Table 1: Main plasma-chemical reactions in the pure nitrogen afterglow.

Reaction number	Reaction	Rate coefficient	Reference
(1)	$N(^4S) + N(^4S) + N_2 \rightarrow N_2(A) + N_2$	$k_1 = 1.05 \cdot 10^{-13}$ cm^3 s^{-1}	[22]
(2)	$N(^4S)$ + wall $\rightarrow N_2$ + wall	k_2 = see text	
(3)	$N_2(A) + N(^4S) \rightarrow N_2(X) + N(^2P)$	$k_3 = 5 \cdot 10^{-11}$ cm^3 s^{-1}	[23]
(4)	$N(^2P) + N_2 \rightarrow N(^2D) + N_2$	$k_4 = 2 \cdot 10^{-18}$ cm^3 s^{-1}	[24]
(5)	$N(^2P) + N \rightarrow N(^2D) + N$	$k_5 = 1.8 \cdot 10^{-12}$ cm^3 s^{-1}	[25]
(6)	$N(^2D) + N_2 \rightarrow N(^4S) + N_2$	$k_6 = 6 \cdot 10^{-15}$ cm^3 s^{-1}	[26]
(7)	$N_2(A) + N_2(A) \rightarrow N_2(C) + N_2$	$k_7 = 2 \cdot 10^{-12}$ cm^3 s^{-1}	[27]

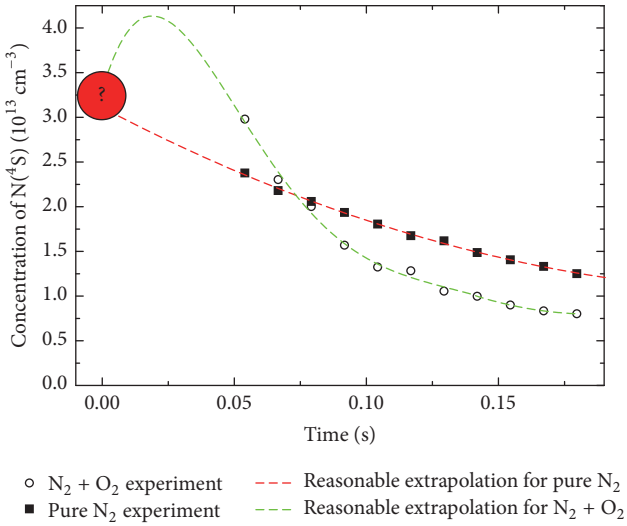

Figure 5: Data from the previous figure recalculated from distance to time. The rough estimation of initial [N] value at $t = 0$ s is shown, too. The sketch of a reasonable time evolution is shown by dashed lines.

it effectively sets the probable shapes of both curves (with and without oxygen admixture) in the unmeasurable region. These are shown in Figure 5 using the dashed lines. One can see that the case without oxygen admixture should be simply governed by losses while the case with oxygen admixture initially exhibits some process producing the nitrogen atoms and only later the losses dominate. Higher losses of N with O_2 present cause the steeper descent of this curve and so both curves intersect.

3.2. Kinetic Modelling of Plasma Afterglow in Pure Nitrogen. The model is based on collisional processes between the principal species in the nitrogen afterglow: N_2 molecules, electronically excited molecules $N_2(A)$, atoms N(S), N(P), and N(D), and it takes into account also the wall processes. The model is focused on $N(^4S)$ and so the species $N_2(X,v)$ despite being another important energy carrier is not included as it cannot directly cause N_2 dissociation and it does not exhibit very strong quenching by nitrogen atoms (which $N_2(A)$ does). An overview of the main plasma-chemical processes based on [28] is presented in Table 1.

The kinetic equations describing the processes in Table 1 were transformed to a set of differential equations and solved numerically using the Euler method. As this method might be unstable for rapidly changing functions, it is necessary to use sufficiently small time-step. This convergence was verified in the presented model. Some parameters, such as k_2 and initial concentrations of $N(^4S)$ and $N_2(A)$, are a priori unknown and must be determined by fitting to the experimental data. The concentration of molecular nitrogen $[N_2] = 2.77 \cdot 10^{19}$ cm^{-3} at standard pressure and temperature was used as one of initial values.

The reaction (1) describes the volume recombination and the reaction (2) the wall recombination of atomic nitrogen in ground state $N(^4S)$. The model includes the reactions of the $N(^2P)$, $N(^2D)$, and $N_2(A)$ metastables, too. However, significant simplifications are possible. In the experiment, only the $N(^4S)$ concentration is actually measured. Moreover, the metastable N atoms generally end in ground state (reactions (4)–(6)). So the reaction (3) effectively produces one $N(^4S)$ atom and is equivalent to $N_2(A)$ deexcitation.

Further simplification stems from the mutual ratio of $[N_2(A)]$ and $[N(^4S)]$. Although these values are a priori unknown, they can be roughly estimated. A rough estimation of the initial concentration $[N_2(A)]_0$ of 10^{11} cm^{-3} can be taken from papers [65–67], which used sufficiently similar conditions to the present ones (atmospheric pressure nitrogen afterglow operated in similar tube diameter and similar input power). As the visual extrapolation of pure nitrogen curve (red hollow diamonds) in Figure 5 gives the initial value of $[N(^4S)]_0$ around 10^{13} cm^{-3}, one may safely assume that $[N(^4S)]_0 > [N_2(A)]_0$.

Using these simplifications, the "full" model of Table 1 is effectively reduced to the set of kinetic equations (1), (2), (3), and (7). The relative difference $\delta = ([N(^4S)]|_{\text{reduced model}} - [N(^4S)]|_{\text{full model}})/[N(^4S)]|_{\text{reduced model}}$ between the reduced and full models is shown in Figure 6 for different initial ratios of $[N(^4S)]$ and $[N_2(A)]$.

In the first few milliseconds there is a big difference between the full and the reduced models due to the reaction (3). But in later reaction times, in which the real experiment is carried out (as discussed above, due to experimental constraints it is not possible to measure at afterglow positions before 0.06 s), there is nearly negligible difference between the full and the reduced models. Taking into account the experimental error around 10% and an assumption about initial values 10^{11} cm^{-3} $< [N_2(A)]_0 < [N(^4S)]_0$, one can safely use the reduced model only.

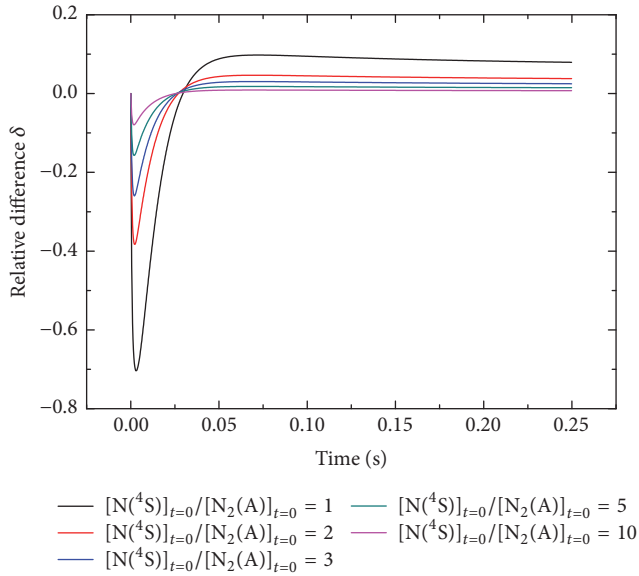

FIGURE 6: Relative difference δ between full (see (1)–(7)) and reduced (see (1), (2), (3), and (7)) models for several initial ratios between $[N(^4S)]$ and $[N_2(A)]$.

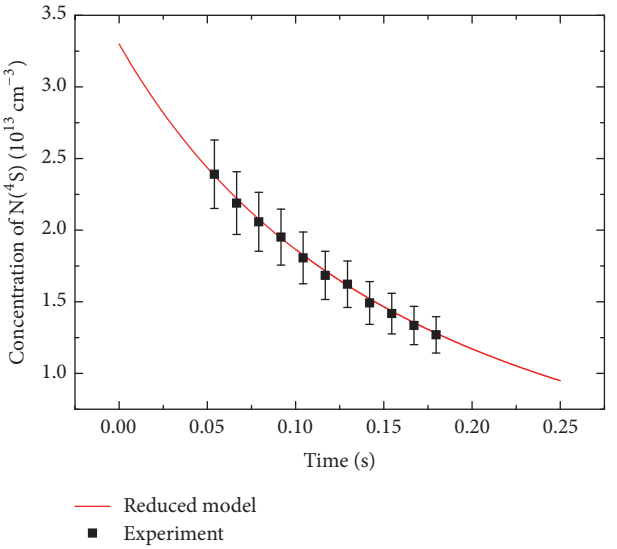

FIGURE 7: Fit of the kinetic model of the pure nitrogen afterglow given by reduced reactions from Table 1 to the experimental data, giving the previously unknown initial value $[N(^4S)]_0 = 3.3 \cdot 10^{13}$ cm^{-3} and the value of k_2.

The least squares fit of experimental data by this reduced model is shown in Figure 7 and gives the values of previously unknown parameters: $[N(^4S)]_0 = 3.3 \cdot 10^{13}$ cm^{-3} and $k_2 = 3.1\,s^{-1}$. To the rate constant k_2 exists corresponding coefficient (probability) of surface recombination/reassociation $\gamma = 1.24 \cdot 10^{-6}$ which is in good agreement with [68] where they get $\gamma_{lit} = 1.35 \cdot 10^{-6}$. Following the reasoning of the previous paragraph, one may assume that these values do not strongly depend (see Figure 6) on the initial concentration of $N_2(A)$ (for sufficiently small $[N_2(A)]_0$).

3.3. Kinetic Modelling of Nitrogen Afterglow with Oxygen Admixture. There are many published sets of kinetic processes for N_2-O_2 mixtures with varying degree of detail [16, 28, 53–56, 69–72]. Taking into account the time scales and typical values of concentrations, these extensive sets can be substantially reduced and simplified. Essentially, it is possible to extend the model of pure nitrogen afterglow (see reactions (1)–(7)) by including $N_2(X,v)$, O_2, O, NO, NO_2, and N_2O (see Table 2).

The inclusion of vibrationally excited nitrogen molecules is necessary as these have even greater importance [73] in $N_2 + O_2$ plasma afterglow. In a nitrogen pink afterglow the vibrationally excited molecules carry a significant part of energy in the afterglow [74, 75]. This energy is then responsible for the formation of $N_2(A)$, $N_2(a')$ and finally for the ionisation of N_2 molecules. Although the pink afterglow was not observed [76] in atmospheric pressure plasma, one may assume [73, 77] the concentration of $N_2(v = 12)$ greater than $5 \cdot 10^{13}$ cm^{-3} at afterglow position of 15 ms.

The concentration of molecular oxygen $[O_2] = 1.56 \cdot 10^{16}$ cm^{-3} is calculated according to the ideal gas law from the experimental conditions (625 ppm of O_2 in N_2 at atmospheric pressure and room temperature).

The reaction set of Table 2 can be further reduced as follows. Kinetic reaction (22) is negligible to the reaction (12) because k_{22} is about two orders of magnitude smaller than k_{12}. For the same reason, reaction (15) can be neglected with respect to reaction (14). Furthermore, (26), according to the numerical calculations, has not significant influence on the concentration of $N(^4S)$, so it can be omitted, too.

Most of the equations describe the loss of ground state metastable atom $N(^4S)$. Equation (13) describes production of $N(^4S)$ but its contribution is not significant in comparison with the losses due to reactions (8), (9), and (10). This is in contrast with the experiment, where an increase in $N(^4S)$ concentration is observed when oxygen is added. Using the larger equation set of [28] does not help either. To explain the $[N(^4S)]$ increase, (23) is needed, where vibrationally excited molecule in the electronic ground state $N_2(X,v)$ produces N atom and nitric oxide molecule by reacting with oxygen atom [69, 77].

The heterogeneous reactions in the model include the wall deexcitation of $N_2(X,v)$, see (24), and $N_2(A)$, see (25).

As usual, the kinetic model must be supplemented by the initial concentrations. The initial value of $[N(^4S)]_0$ was taken from the pure nitrogen model. Due to the adsorption of oxygen on the walls of the afterglow tube [78–81], a smaller value of the wall recombination coefficient k_2 (change from $3.1\,s^{-1}$ to $0.5\,s^{-1}$) was assumed. Atomic oxygen wall recombination coefficient k_{16} was considered to be same as k_2 for simplicity. Rate constants for wall deexcitation (24) and (25) were taken to be the same for both species, that is, $k_{24} = k_{25}$, with estimated value in range of 1–10 s^{-1} to correspond to [82]. The precise value of k_{24} and k_{25} is calculated by fitting the model to the experimental data.

The final simplified set of equations considered in the reduced model of N_2-O_2 afterglow consists of (1)–(3), (7)–(14), (16)–(21), and (23)–(25). The remaining unknowns

Table 2: Additional set of kinetic reactions for nitrogen afterglow with oxygen admixture, mostly based on [28].

Reaction number	Reaction	Rate coefficient	Reference
(8)	$N + O_2 \rightarrow NO + O$	$k_8 = 1.03 \cdot 10^{-16}$ cm^3 s^{-1}	[22]
(9)	$N + O + N_2 \rightarrow NO + N_2$	$k_9 = 2.74 \cdot 10^{-13}$ cm^3 s^{-1}	[22]
(10)	$N + NO \rightarrow N_2 + O$	$k_{10} = 1.82 \cdot 10^{-13}$ cm^3 s^{-1}	[22]
(11)	$O + NO + N_2 \rightarrow NO_2 + N_2$	$k_{11} = 9.54 \cdot 10^{-13}$ cm^3 s^{-1}	[22]
(12)	$N_2(A) + O_2 \rightarrow N_2(X) + O + O$	$k_{12} = 2.54 \cdot 10^{-12}$ cm^3 s^{-1}	[23]
(13)	$N_2(A) + O \rightarrow NO + N(^2D) \rightarrow NO + N(^4S)$	$k_{13} = 7 \cdot 10^{-12}$ cm^3 s^{-1}	[29]
(14)	$O + O + N_2 \rightarrow O_2 + N_2$	$k_{14} = 7.91 \cdot 10^{-14}$ cm^3 s^{-1}	[28]
(15)	$O + O + O_2 \rightarrow 2O_2$	$k_{15} = 1{,}05 \cdot 10^{-16}$ cm^3 s^{-1}	[28]
(16)	$O + \text{wall} \rightarrow O_2 + \text{wall}$	k_{16} = see text	
(17)	$N + NO_2 \rightarrow N_2 + O_2$	$k_{17} = 7 \cdot 10^{-13}$ cm^3 s^{-1}	[28]
(18)	$N + NO_2 \rightarrow N_2 + O + O$	$k_{18} = 9.1 \cdot 10^{-13}$ cm^3 s^{-1}	[28]
(19)	$N + NO_2 \rightarrow N_2O + O$	$k_{19} = 3 \cdot 10^{-12}$ cm^3 s^{-1}	[28]
(20)	$N + NO_2 \rightarrow 2NO$	$k_{20} = 2.3 \cdot 10^{-12}$ cm^3 s^{-1}	[28]
(21)	$O + NO_2 \rightarrow NO + O_2$	$k_{21} = 2.54 \cdot 10^{-12}$ cm^3 s^{-1}	[28]
(22)	$N_2(A) + O_2 \rightarrow N_2O + O$	$k_{22} = 7.8 \cdot 10^{-14}$ cm^3 s^{-1}	[23]
(23)	$N_2(X,v) + O \rightarrow NO + N$	k_{23} = see text	
(24)	$N_2(X,v) + \text{wall} \rightarrow N_2 + \text{wall}$	k_{24} = see text	
(25)	$N_2(A) + \text{wall} \rightarrow N_2 + \text{wall}$	k_{25} = see text	
(26)	$NO_2 + NO_2 + N_2 \rightarrow N_2O_4 + N_2$	$k_{26} = 5.64 \cdot 10^{-13}$ cm^3 s^{-1}	[22]

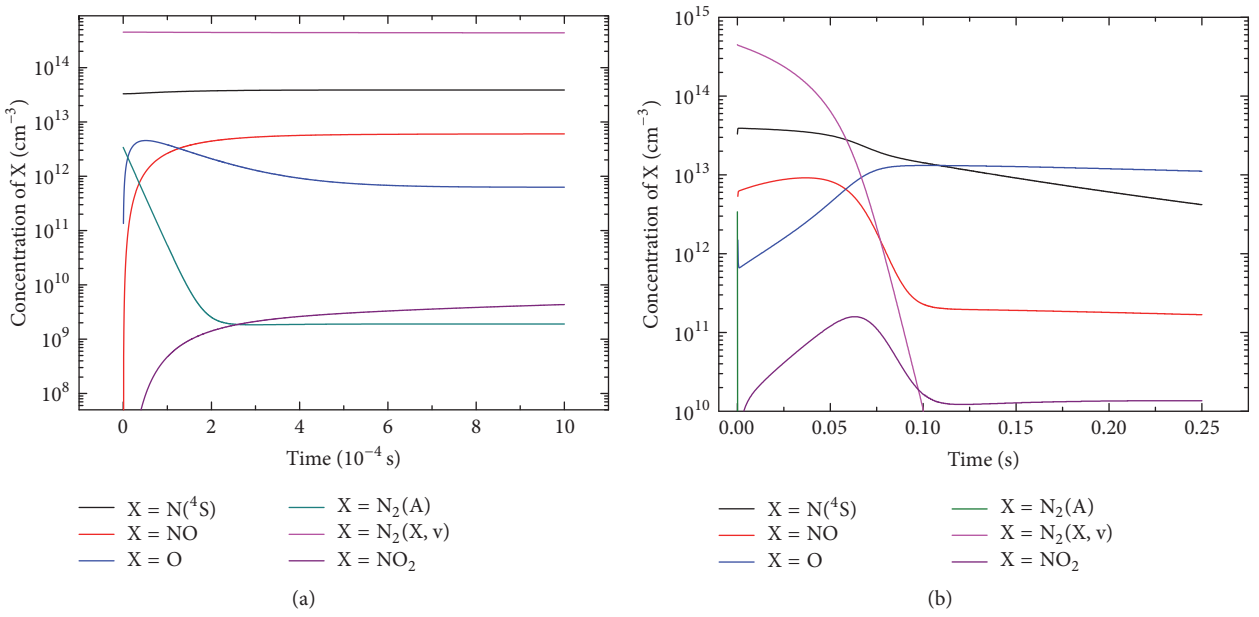

Figure 8: The temporal evolution of main species considered in the reduced kinetic model of N_2-O_2 afterglow. For clarity, the data are shown in two time scales.

are the initial concentrations of $N_2(A)$, $N_2(X,v)$ and the rate constants k_{23}, k_{24}, and k_{25}. These parameters were determined from the least squares fit of model to the experimental data.

Figure 8 shows the calculated temporal evolution of concentrations of main species considered in the present model in short (a) and long (b) time scales. The dominant species (besides the parent N_2 and O_2) are the nitrogen and oxygen atoms. Interestingly, despite the very unfavourable ratio of $[O_2]/[N_2] = 625$ ppm, there are more oxygen atoms than nitrogen atoms in the late afterglow. Electronically and vibrationally excited nitrogen molecules disappear quickly. Both oxides of nitrogen, nitrogen dioxide NO_2 and nitric oxide NO, remain after 0.1 s constant, [NO] being approx. 10 times higher than $[NO_2]$.

Full comparison of the model and the experiment is shown in Figure 9 for both cases, with and without the oxygen admixture. Values of a priori unknown parameters obtained

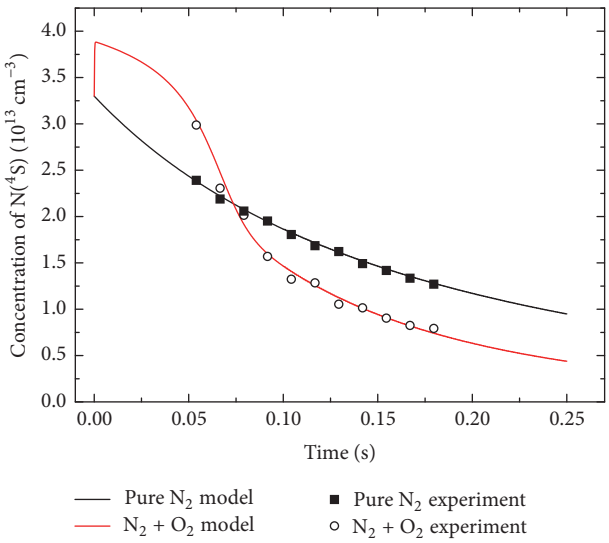

FIGURE 9: The parameters from the fit are used to calculate the extrapolation to shorter afterglow times of kinetic models of atmospheric pressure nitrogen afterglow with and without oxygen admixture.

by the fit of N_2-O_2 model are $[N_2(A)]_0 = 3.4 \cdot 10^{12}$ cm^{-3}, $[N_2(X, v)]_0 = 4.5 \cdot 10^{14}$ cm^{-3}, $k_{23} = 1.6 \cdot 10^{-11}$ cm^3 s^{-1}, and $k_{24} = k_{25} = 8.7$ s^{-1}. The value of k_{23} obtained from the fit is in very good agreement with [16] where this constant was estimated to be at least 10^{-11} cm^3 s.

The agreement between the models and the experimental data in Figure 9 is very good. Moreover, the model covers also the times shorter than 50 ms which are inaccessible by the experiment. The effect of initially increased [N] just after oxygen admixture, which was predicted in Figure 5, is therefore verified and explained by reaction of vibrationally excited N_2(X,v) with atomic oxygen.

4. Conclusions

Quantitative electron spin/paramagnetic resonance spectroscopy was used to measure the concentration of nitrogen atoms in flowing atmospheric pressure dielectric barrier discharge afterglow with typical [N] values around $2 \cdot 10^{13}$ cm^{-3}. The evolution of this concentration along the afterglow tube was shown to be significantly affected by the relatively small amount (625 ppm) of oxygen added into the early afterglow. The nitrogen dissociation is increased just after the oxygen inlet and it is decreased in later parts of the afterglow.

Numerical kinetic model explains this behaviour by a balance of production and loss terms, both of which are affected by the presence of oxygen. Main reaction producing N atoms is the collision of N_2(X,v) with oxygen atoms. By fitting the model to the experimental data, it was possible to estimate several a priori unknown and not directly measurable quantities, such as the initial concentrations of N(^{4}S), N_2(A), and N_2(X,v), wall recombination coefficient of N atoms, and rate coefficient of some reactions.

Competing Interests

The authors declare that they have no competing interests.

Acknowledgments

This research has been supported by the Project LO1411 (NPU I) funded by Ministry of Education, Youth and Sports of Czech Republic.

References

[1] B. Eliasson, M. Hirth, and U. Kogelschatz, "Ozone synthesis from oxygen in dielectric barrier discharges," *Journal of Physics D: Applied Physics*, vol. 20, no. 11, pp. 1421–1437, 1987.

[2] J. P. Boeuf, "Plasma display panels: physics, recent developments and key issues," *Journal of Physics D: Applied Physics*, vol. 36, no. 6, pp. R53–R79, 2003.

[3] M. Strobel, C. S. Lyons, and K. Mittal, Eds., *Plasma Surface Modification of Polymers: Relevance to Adhesion*, VSP, 1994.

[4] U. Kogelschatz, "Dielectric-barrier discharges: their history, discharge physics, and industrial applications," *Plasma Chemistry and Plasma Processing*, vol. 23, no. 1, pp. 1–46, 2003.

[5] L. M. Zhou, B. Xue, U. Kogelschatz, and B. Eliasson, "Nonequilibrium plasma reforming of greenhouse gases to synthesis gas," *Energy & Fuels*, vol. 12, no. 6, pp. 1191–1199, 1998.

[6] L. Zajíčková, M. Eliáš, O. Jašek et al., "Atmospheric pressure microwave torch for synthesis of carbon nanotubes," *Plasma Physics and Controlled Fusion*, vol. 47, no. 12, pp. B655–B666, 2005.

[7] P. Synek, O. Jašek, L. Zajíčková, B. David, V. Kudrle, and N. Pizúrová, "Plasmachemical synthesis of maghemite nanoparticles in atmospheric pressure microwave torch," *Materials Letters*, vol. 65, no. 6, pp. 982–984, 2011.

[8] G. Fridman, G. Friedman, A. Gutsol, A. B. Shekhter, V. N. Vasilets, and A. Fridman, "Applied plasma medicine," *Plasma Processes and Polymers*, vol. 5, no. 6, pp. 503–533, 2008.

[9] G. Fridman, A. D. Brooks, M. Balasubramanian et al., "Comparison of direct and indirect effects of non-thermal atmospheric-pressure plasma on bacteria," *Plasma Processes and Polymers*, vol. 4, no. 4, pp. 370–375, 2007.

[10] J. Heinlin, G. Morfill, M. Landthaler et al., "Plasma medicine: possible applications in dermatology," *JDDG: Journal der Deutschen Dermatologischen Gesellschaft*, vol. 8, no. 12, pp. 968–976, 2010.

[11] V. Stěpánová, P. Slavíček, M. Stupavská, J. Jurmanová, and M. Černák, "Surface chemical changes of atmospheric pressure plasma treated rabbit fibres important for felting process," *Applied Surface Science*, vol. 355, pp. 1037–1043, 2015.

[12] W. A. P. Claassen, W. G. J. N. Valkenburg, M. F. C. Willemsen, and W. M. Wijgert, "Influence of deposition temperature, gas pressure, gas phase composition, and RF frequency on composition and mechanical stress of plasma silicon nitride layers," *Journal of the Electrochemical Society*, vol. 132, no. 4, pp. 893–898, 1985.

[13] G. G. Tibbetts, "Role of nitrogen atoms in 'ion–nitriding'," *Journal of Applied Physics*, vol. 45, no. 11, pp. 5072–5073, 1974.

[14] A. Fridman, *Plasma Chemistry*, Cambridge University Press, 2008.

[15] I. Stefanovic, N. K. Bibinov, A. A. Deryugin, I. P. Vinogradov, A. P. Napartovich, and K. Wiesemann, "Kinetics of ozone and

nitric oxides in dielectric barrier discharges in O_2/NO_x and $N_2/O_2/NO_x$ mixtures," *Plasma Sources Science and Technology*, vol. 10, no. 3, p. 406, 2001.

[16] V. Guerra and J. Loureiro, "Non-equilibrium coupled kinetics in stationary N_2-O_2 discharges," *Journal of Physics D: Applied Physics*, vol. 28, no. 9, pp. 1903–1918, 1995.

[17] S. Tada, S. Takashima, M. Ito, M. Hori, T. Goto, and Y. Sakamoto, "Measurement and control of absolute nitrogen atom density in an electron-beam-excited plasma using vacuum ultraviolet absorption spectroscopy," *Journal of Applied Physics*, vol. 88, no. 4, pp. 1756–1759, 2000.

[18] P. Vašina, V. Kudrle, A. Tálský, P. Botoš, M. Mrázková, and M. Meško, "Simultaneous measurement of N and O densities in plasma afterglow by means of NO titration," *Plasma Sources Science and Technology*, vol. 13, no. 4, pp. 668–674, 2004.

[19] S. Agarwal, B. Hoex, M. C. M. Van de Sanden, D. Maroudas, and E. S. Aydil, "Absolute densities of N and excited N_2 in a N_2 plasma," *Applied Physics Letters*, vol. 83, no. 24, pp. 4918–4920, 2003.

[20] J. Amorim, G. Baravian, and J. Jolly, "Laser-induced resonance fluorescence as a diagnostic technique in non-thermal equilibrium plasmas," *Journal of Physics D: Applied Physics*, vol. 33, no. 9, pp. R51–R65, 2000.

[21] F. Gaboriau, U. Cvelbar, M. Mozetic, A. Erradi, and B. Rouffet, "Comparison of TALIF and catalytic probes for the determination of nitrogen atom density in a nitrogen plasma afterglow," *Journal of Physics D: Applied Physics*, vol. 42, no. 5, Article ID 055204, 2009.

[22] O. E. Krivonosova, S. A. Losev, V. P. Nalivaiko, Y. K. Mukoseev, and O. P. Shatalov, *Plasma Chemistry*, vol. 14 of *edited by B. M. Smirnov*, Energoatomizdat, Moscow, Russia, 1987.

[23] M. P. Iannuzi, J. B. Jeffries, and F. Kaufman, "Product Channels of the N_2 $(A^3\Sigma_u^+)$ + O_2 interaction," *Chemical Physics Letters*, vol. 87, no. 6, pp. 570–574, 1982.

[24] R. J. Donovan and D. Husain, "Recent advances in the chemistry of electronically excited atoms," *Chemical Reviews*, vol. 70, no. 4, pp. 489–516, 1970.

[25] D. I. Slovetskii, *Mechanisms of Chemical Reactions in Nonequilibrium Plasma*, Mir, Moscow, Russia, 1980 (Russian).

[26] M. H. Bortner and T. Bauer, *Defense Nuclear Agency Reaction Rate Handbook*, DNA 1948H, US GPO, Washington, DC, USA, 1971.

[27] V. P. Silakov, *Mechanism of Supporting the Long-Lived Plasma in Molecular Nitrogen at High Pressure*, 010-90M, Moscow Engineering Physical Institute, 1990.

[28] I. A. Kossyi, A. Y. Kostinsky, A. A. Matveyev, and V. P. Silakov, "Kinetic scheme of the non-equilibrium discharge in nitrogen-oxygen mixtures," *Plasma Sources Science and Technology*, vol. 1, no. 3, 1992.

[29] L. G. Piper, "The excitation of O(1S) in the electronic energy transfer between N2(A3S+ u) and O," *The Journal of Chemical Physics*, vol. 77, pp. 2373–2377, 1982.

[30] E. K. Zavoisky, "Paramagnetic relaxation of liquid solutions for perpendicular fields," *Journal of Physics-USSR*, vol. 9, pp. 211–216, 1945.

[31] E. K. Zavoisky, "Spin-magnetic resonance in paramagnetics," *Journal of Physics-USSR*, vol. 9, pp. 211–245, 1945.

[32] E. K. Zavoisky, "Spin magnetic resonance in the decimeter-wave region," *Journal of Physics-USSR*, vol. 10, pp. 197–198, 1946.

[33] A. Carrington and A. D. McLachlan, *Introduction to Magnetic Resonance with Applications to Chemistry and Chemical Physics*, Harper and Row, New York, NY, USA, 1967.

[34] C. P. Poole, *Electron Spin Resonance*, John Wiley & Sons, New York, NY, USA, 2nd edition, 1983.

[35] J. A. Well and J. R. Bolton, *Electron Paramagnetic Resonance*, John Wiley & Sons, New York, NY, USA, 2007.

[36] A. Abragam and J. H. Van Vleck, "Theory of the microwave Zeeman effect in atomic oxygen," *Physical Review*, vol. 92, no. 6, pp. 1448–1455, 1953.

[37] M. Tinkham and M. W. P. Strandberg, "Theory of the fine structure of the molecular oxygen ground state," *Physical Review*, vol. 97, no. 4, pp. 937–950, 1955.

[38] S. Krongelb and M. W. P. Strandberg, "Use of paramagnetic-resonance techniques in the study of atomic oxygen recombinations," *The Journal of Chemical Physics*, vol. 31, no. 5, pp. 1196–1210, 1959.

[39] T. K. Ishii, *Handbook of Microwave Technology: Applications*, Academic Press, New York, NY, USA, 1995.

[40] P. Zeeman, "Over den invloed fleener magnetisatie op den aard van het door een stof uitgezonden licht," *Verslagen Der Koninklijke Akademie van Wetenschappen te Amsterdam*, vol. 5, p. 181, 1896.

[41] A. A. Westenberg and N. Dehaas, "Observations on ESR linewidths and concentration measurements of gas–phase radicals," *The Journal of Chemical Physics*, vol. 51, no. 12, pp. 5215–5225, 1969.

[42] T. J. Cook and T. A. Miller, "Gas-phase EPR linewidths and intermolecular potentials. I. Theory," *The Journal of Chemical Physics*, vol. 59, no. 3, pp. 1342–1351, 1973.

[43] A. A. Westenberg, "Use of ESR for the quantitative determination of gas phase atom and radical concentrations," *Progress in Reaction Kinetics*, vol. 7, pp. 23–82, 1973.

[44] A. A. Westenberg and N. De Haas, "Quantitative measurements of gas phase O and N Atom concentrations by ESR," *The Journal of Chemical Physics*, vol. 40, no. 10, pp. 3087–3098, 1964.

[45] T. J. Cook, B. R. Zegarski, W. H. Breckenridge, and T. A. Miller, "Gas phase EPR of vibrationally excited O_2," *The Journal of Chemical Physics*, vol. 58, no. 4, pp. 1548–1552, 1973.

[46] W. H. Breckenridge and T. A. Miller, "Detection of metastable 3P argon atoms by gas phase EPR," *Chemical Physics Letters*, vol. 12, no. 3, pp. 437–442, 1972.

[47] V. Doležal, M. Mrázková, P. Dvořák, A. Tálský, and V. Kudrle, "Hydrogen line broadening in afterglow observed by means of EPR," *Acta Physica Slovaca*, vol. 55, no. 5, pp. 435–439, 2005.

[48] V. Kudrle, A. Tálský, A. Kudláč, V. Křápek, and J. Janča, "Influence of admixtures on production rate of atomic nitrogen," *Czechoslovak Journal of Physics*, vol. 50, no. 3, pp. 305–308, 2000.

[49] P. Dvořák, V. Doležal, M. Mrázková, V. Kudrle, A. Tálský, and J. Janča, "EPR measurements in hydrogen post-discharge," *Czechoslovak Journal of Physics*, vol. 54, no. 3, pp. C539–C543, 2004.

[50] V. Kudrle, P. Vašina, A. Tálský, and J. Janča, "Measurement of concentration of N atoms in afterglow," *Czechoslovak Journal of Physics*, vol. 52, pp. 589–595, 2002.

[51] V. Kudrle, P. Vašina, A. Tálský, M. Mrázková, O. Štec, and J. Janča, "Plasma diagnostics using electron paramagnetic resonance," *Journal of Physics D: Applied Physics*, vol. 43, no. 12, Article ID 124020, 2010.

[52] C. D. Pintassilgo, V. Guerra, O. Guaitella, and A. Rousseau, "Study of gas heating mechanisms in millisecond pulsed discharges and afterglows in air at low pressures," *Plasma Sources Science and Technology*, vol. 23, no. 2, Article ID 025006, 2014.

[53] C. D. Pintassilgo, O. Guaitella, and A. Rousseau, "Heavy species kinetics in low-pressure dc pulsed discharges in air," *Plasma Sources Science and Technology*, vol. 18, no. 2, Article ID 025005, 2009.

[54] A. Ricard, S. G. Oh, and V. Guerra, "Line-ratio determination of atomic oxygen and metastable absolute densities in an RF nitrogen late afterglow," *Plasma Sources Science and Technology*, vol. 22, no. 3, Article ID 035009, 2013.

[55] M. Mrázková, P. Vašina, V. Kudrle, A. Tálský, C. D. Pintassilgo, and V. Guerra, "On the oxygen addition into nitrogen post-discharges," *Journal of Physics D: Applied Physics*, vol. 42, no. 7, Article ID 075202, 2009.

[56] A. A. Westenberg, "Intensity relations for determining gas–phase OH, Cl, Br, I, and free–electron concentrations by quantitative ESR," *The Journal of Chemical Physics*, vol. 43, no. 5, pp. 1544–1549, 1965.

[57] W. Siemens, "Ueber die elektrostatische induction und die verzögerung des stroms in flaschendrähten," *Annalen der Physik*, vol. 178, no. 9, pp. 66–122, 1857.

[58] S. P. Sutera and R. Skalak, "The history of Poiseuille's law," *Annual Review of Fluid Mechanics*, vol. 25, no. 1, pp. 1–20, 1993.

[59] A. Roth, *Vacuum Technology*, Elsevier, 2012.

[60] J. M. Gershenzon, A. B. Nalbandyan, and V. B. Rozenshtein, *Magnetic Resonance in Gases*, Publishing House of Academy of Sciences of Armenian Soviet Socialist Republic, 1987.

[61] A. Tálský and M. Kunovský, "Die dissoziation des stickstoffen in der mikrowellen entladung," *Scripta Facultatis Scientiarum Naturalium, Universitatis Purkynianae Brunensis Physica*, vol. 18, no. 6, article 229, 1988.

[62] O. Reynolds, "An experimental investigation of the circumstances which determine whether the motion of water shall be direct or sinuous, and of the law of resistance in parallel channels," *Philosophical Transactions of the Royal Society of London*, vol. 174, no. 0, pp. 935–982, 1883.

[63] J. Kestin and W. Leidenfrost, "An absolute determination of the viscosity of eleven gases over a range of pressures," *Physica*, vol. 25, no. 7–12, pp. 1033–1062, 1959.

[64] M. Ohmi and M. Iguchi, "Critical Reynolds number in an oscillating pipe flow," *Bulletin of JSME*, vol. 25, no. 200, pp. 165–172, 1982.

[65] A.-M. Pointu, A. Ricard, E. Odic, and M. Ganciu, "Nitrogen atmospheric pressure post discharges for surface biological decontamination inside small diameter tubes," *Plasma Processes and Polymers*, vol. 5, no. 6, pp. 559–568, 2008.

[66] A. M. Pointu, E. Mintusov, and P. Fromy, "Study of an atmospheric pressure flowing afterglow in N_2/NO mixture and its application to the measurement of $N_2(A)$ concentration," *Plasma Sources Science and Technology*, vol. 19, no. 1, Article ID 015018, 2009.

[67] A. M. Pointu and G. D. Stancu, "$N_2(A)$ as the source of excited species of N_2, N and O in a flowing afterglow of N_2/NO mixture at atmospheric pressure," *Plasma Sources Science and Technology*, vol. 20, no. 2, Article ID 025005, 2011.

[68] V. Mazánková, D. Trunec, and F. Krčma, "Study of nitrogen flowing afterglow with mercury vapor injection," *Journal of Chemical Physics*, vol. 141, no. 15, Article ID 154307, 2014.

[69] B. F. Gordiets, C. M. Ferreira, V. L. Guerra et al., "Kinetic model of a low-pressure N_2-O_2 flowing glow discharge," *IEEE Transactions on Plasma Science*, vol. 23, no. 4, pp. 750–768, 1995.

[70] G. Cartry, L. Magne, and G. Cernogora, "Experimental study and modelling of a low-pressure N_2-O_2 time afterglow," *Journal of Physics D: Applied Physics*, vol. 32, no. 15, pp. 1894–1907, 1999.

[71] C. D. Pintassilgo, J. Loureiro, and V. Guerra, "Modelling of a N_2–O_2 flowing afterglow for plasma sterilization," *Journal of Physics D: Applied Physics*, vol. 38, no. 3, 2005.

[72] W. Van Gaens and A. Bogaerts, "Kinetic modelling for an atmospheric pressure argon plasma jet in humid air," *Journal of Physics D: Applied Physics*, vol. 46, no. 27, Article ID 275201, 2013.

[73] D. Blois, P. Supiot, M. Barj et al., "The microwave source's influence on the vibrational energy carried by in a nitrogen afterglow," *Journal of Physics D: Applied Physics*, vol. 31, no. 19, article 2521, 1998.

[74] J. Loureiro, P. A. Sá, and V. Guerra, "Role of long-lived N2($X^1\Sigma g+$,v) molecules and N2($A3\Sigma u+$) and N2(a'$1\Sigma u-$) states in the light emissions of an N2 afterglow," *Journal of Physics D: Applied Physics*, vol. 34, no. 12, pp. 1769–1778, 2001.

[75] N. Sadeghi, C. Foissac, and P. Supiot, "Kinetics of $N_2(A^3 \sum_u^+)$ molecules and ionization mechanisms in the afterglow of a flowing N_2 microwave discharge," *Journal of Physics D: Applied Physics*, vol. 34, no. 12, pp. 1779–1788, 2001.

[76] A.-M. Pointu, A. Ricard, B. Dodet, E. Odic, J. Larbre, and M. Ganciu, "Production of active species in N_2-O_2 flowing post-discharges at atmospheric pressure for sterilization," *Journal of Physics D: Applied Physics*, vol. 38, no. 12, pp. 1905–1909, 2005.

[77] M. Capitelli, C. M. Ferreira, B. F. Gordiets, and A. I. Osipov, *Plasma Kinetics in Atmospheric Gases*, vol. 31, Springer Science & Business Media, 2013.

[78] V. Zvonicek, V. Guerra, J. Loureiro, A. Talsky, and M. Touzeau, "Surface and volume kinetics of O(3P) atoms in a low-pressure O2-N2 microwave discharge," in *Proceedings of the 23rd International Conference on Phenomena in Ionized Gases (ICPIG '97)*, vol. 4, p. 160, Toulouse, France, July 1997.

[79] G. Cartry, L. Magne, G. Cernogora, M. Touzeau, and M. Vialle, "Effect of wall treatment on oxygen atoms recombination," in *Proceedings of the 23rd International Conference on Phenomena in Ionized Gases (ICPIG '97)*, vol. 2, pp. 70–71, Toulouse, France, July 1997.

[80] G. Cartry, L. Magne, and G. Cernogora, "Atomic oxygen recombination on fused silica: modelling and comparison to low-temperature experiments (300 K)," *Journal of Physics D: Applied Physics*, vol. 33, no. 11, 2000.

[81] K. M. Evenson and D. S. Burch, "Atomic–nitrogen recombination," *The Journal of Chemical Physics*, vol. 45, no. 7, pp. 2450–2460, 1966.

[82] G. Black, H. Wise, S. Schechter, and R. L. Sharpless, "Measurements of vibrationally excited molecules by Raman scattering. II. Surface deactivation of vibrationally excited N_2," *The Journal of Chemical Physics*, vol. 60, no. 9, pp. 3526–3536, 1974.